Quantitative prediction model for lithium-ion battery life uncertainty based on DAE-CNN-BiGRU quantile regression

Shengli Wu[1], Dan Li[1], Wenting Xing[2], Ying Liu[3]

[1]College of Traffic and Transportation, Chongqing Jiaotong University, Chongqing, 400074, People's Republic of China

[2]School of Management Science and Engineering, Chongqing Technology and Business University, Chongqing 400067, People's Republic of China

[3]School of Engineering, Cardiff University, Cardiff, CF24 3AA, UK

Abstract: To ensure the safety and reliability of lithium-ion battery management systems (BMS), accurately predicting the remaining useful life (RUL) is essential. However, during the operation of lithium-ion batteries, various uncertainties, including energy regeneration and localized fluctuations, introduce significant challenges, making it difficult to predict RUL with the desired accuracy. In this paper, we develop a quantitative model for predicting the uncertainty in the remaining life of lithium-ion batteries. To be specific, the approach begins by employing a denoising auto-encoder (DAE) to reconstruct the original signal during data preprocessing. Next, a one-dimensional convolutional neural network (1D-CNN) is utilized to deeply analyze the capacity data of the lithium-ion batteries. The representative features extracted by the CNN are then fed into a bidirectional gated recurrent unit (BiGRU) network. A quantile regression (QR) layer is integrated into the BiGRU architecture to generate the final predictions of the battery's remaining service life. The quantile regression loss function is applied during the network training process to enhance the accuracy of the remaining service life predictions. Performance evaluation was conducted using publicly available datasets from NASA and CALCE, with comparisons against other prediction methods. Experimental results indicate that the quantile regression approach enhances the accuracy of the gated recurrent unit (GRU) neural network, demonstrating superior predictive performance.

Keywords: lithium-ion battery; denoising auto-encoder; convolutional neural network; bi-directional cyclic gating unit; remaining service life prediction.

1 Introduction

Lithium-ion batteries are extensively used in electric vehicles and energy storage systems due to their high specific energy, long service life, low self-discharge rate, and environmental friendliness [1]. As the number of charge and discharge cycles increases, chemical reactions within the lithium-ion battery can cause irreversible aging, resulting in a reduction in battery life. The remaining service life of a battery is a crucial indicator of its aging status [2], and accurately predicting it is vital for the operational safety of energy storage systems. However, factors such as temperature variations, the number of charge and discharge cycles, load changes, and other internal and external influences complicate the precise estimation of the battery's remaining service life. Therefore, accurate and reliable prediction of the remaining service life of lithium-ion batteries is essential to ensure their safe and reliable operation.

Currently, there are two general categories for predicting the remaining service life of batteries: model-based methods and data-driven methods [3]. The model-based approach primarily examines the physicochemical properties of the internal materials of lithium-ion batteries by analyzing the degradation mechanisms of electrochemical reactions and battery performance. This method is used to infer the remaining service life of the battery. Liu et al. [4] proposed a method for predicting the remaining useful life (RUL) of lithium-ion batteries based on a particle filtering (PF) framework and an electrochemical model. Their approach involves identifying

parameters of a simplified electrochemical model through a specialized current excitation and then constructing observation equations using these parameters as state variables within the particle filtering algorithm. This method achieves high-quality RUL predictions. Sun et al.[5] introduced the concept of Remaining Chargeable Quantity (RCQ) and employed the Dual Extended Kalman Filter (Dual-ADEKF) algorithm to identify model parameters online. This approach also accounts for the aging inconsistency across lithium-ion battery packs, effectively estimating the usable capacity of aging batteries. Guha et al. [6] modeled internal resistance growth and capacity degradation by utilizing electrochemical impedance spectroscopy (EIS) test data alongside battery capacity test data, achieving predictions of battery remaining useful life (RUL). Chen et al. [7] proposed the ECM-VIT method, which integrates the equivalent circuit model (ECM) of lithium-ion batteries with an improved vision transformer (VIT) to achieve high-precision prediction of the state of health (SOH). Experimental studies have validated the superior performance of this method in SOH estimation. Model-based approaches can effectively elucidate the spatio-temporal dynamics of electrochemical reactions within a battery, which made them particularly favored by researchers in earlier studies. However, the inherent complexity of these electrochemical reactions poses significant challenges, limiting the accuracy of electrochemical modeling.

To overcome these problems, data-driven lifetime prediction methods have gradually become a hot research topic. Data-driven lithium-ion battery life prediction does not require complex battery modeling. Instead, it explores the relationship between external parameters and the internal state of the battery by analyzing and learning from patterns, trends, and correlations within the data. Furthermore, data-driven methods are more straightforward to implement and incur lower computational costs compared to model-based approaches. Consequently, with the advancement of computational performance and continuous innovations in algorithms in recent years, data-driven methods such as artificial neural networks (ANN) [8] [9], support vector machines (SVM) [10][11], long short-term memory (LSTM)[12][13], and convolutional neural networks (CNN) [14], [15] have become mainstream. Bao et al. [16] proposed a hybrid neural network framework (CNN-VLSTM-DA) that integrates a convolutional neural network (CNN), a variant long short-term memory network (VLSTM), and a dimensional attention mechanism. The VLSTM is utilized to capture temporal dependencies, while the attention mechanism assigns different weights to various feature dimensions, thereby enhancing prediction accuracy. This framework enables accurate estimation of the state of health (SOH) of lithium-ion batteries. Liu et al. [17] investigated the aging mechanisms of lithium-ion batteries by examining the three stages of battery degradation through incremental capacity analysis and electrochemical impedance spectroscopy. Finally, they employed a backpropagation neural network optimized by a genetic algorithm to predict the state of health of lithium-ion batteries throughout their total lifespan. Zhai et al. [18] proposed a prediction method based on a gated recurrent unit (GRU) network. This model by extracting capacity data from aging batteries as predictive features, and employed the Tunicate Swarm Algorithm (TSA) to optimize the GRU network. This approach effectively captures the dependency relationships between degradation capacities and achieves RUL prediction. Yu et al. [20] proposed a bi-directional long and short-term memory (BiLSTM) model for predicting the degradation trend of battery capacity, which effectively captured and updated the key information in the capacity degradation data through the ability of the BiLSTM network structure to learn long-term. Additionally, Zhang et al. [20] proposed a rapid multi-fault diagnosis method based on curve Manhattan distance and voltage difference analysis, enabling efficient detection and classification of faults in lithium-ion battery packs. This method offers advantages such as low computational cost and high diagnostic accuracy. Guo et al. [21] employed complementary ensemble empirical mode decomposition with adaptive noise (CEEMDAN) to decompose the data. Subsequently, a neural network combining a convolutional neural network (CNN) and bidirectional long short-term memory (BiLSTM) was utilized to predict the remaining service life of lithium-ion batteries. Zhang et al. [22] combined the strengths of both data-driven and model-based approaches, proposing an interactive method for predicting the remaining useful life (RUL) using Particle Filtering, a Temporal Attention Mechanism, and a Bidirectional Gated Recurrent Unit (PF-BiGRU-TSAM) for data modeling. Lv et al. [23] proposed a highly accurate and reliable method for predicting the remaining useful life (RUL) of lithium-ion

batteries. This approach integrates complementary ensemble empirical mode decomposition with adaptive noise (CEEMDAN) and a convolutional neural network (CNN)-bidirectional gated recurrent unit (BiGRU). Xia et al. [24] tackled the issue of insufficient feature extraction accuracy by employing a specially designed denoising auto-encoder (DAE) to eliminate common noise in lithium-ion battery data. They utilized a convolutional neural network (CNN) to mine correlations among multiple battery features and a self-attentive long short-term memory (LSTM) network to capture time-series information from long-term degradation sequences. This approach enables effective RUL prediction of lithium-ion batteries. Compared to other typical data-driven methods, their method demonstrated higher prediction accuracy and robustness in datasets affected by various types of noise. Although many data-driven prediction methods have been proposed above, the prediction results are mainly focused on the estimation of deterministic points. With the widespread deployment of lithium-ion batteries in applications such as electric vehicles and energy storage systems, the safety risks and economic losses associated with the uncertainty in battery lifetime prediction have become increasingly prominent. Issues such as premature battery replacement and equipment malfunction caused by inaccurate predictions exemplify the negative consequences of this uncertainty. It significantly hampers the ability of existing prediction methods to accurately estimate battery lifespan and poses substantial challenges to the precise decision-making of battery management systems (BMS).

In summary, model-based approaches offer insights into the degradation process by capturing the internal mechanisms of batteries but are constrained by the complexity of modeling. In contrast, data-driven methods have gained significant attention due to their efficiency and flexibility, enabling the analysis of complex operating conditions. However, uncertainties arising from energy regeneration and local fluctuations during lithium-ion battery operation present challenges, highlighting the need for further improvements in uncertainty analysis and predictive accuracy. Based on this, this study proposes a novel uncertainty-quantified prediction model for the remaining useful life (RUL) of lithium-ion batteries. Compared with the aforementioned approaches, the DAE-CNN-BiGRU-QR model proposed in this study establishes a comprehensive and distinctive framework encompassing data denoising, feature extraction, and uncertainty quantification. This integrated approach offers significant advantages in addressing practical challenges. The model combines a one-dimensional convolutional neural network (1D-CNN) with a bidirectional gated recurrent unit (BiGRU). A convolutional layer in the 1D-CNN is employed to extract deep representative features hidden in the original measurement signals, addressing the challenges of complex and inefficient feature selection in traditional methods. Additionally, to characterize the uncertainty in the lithium-ion battery capacity prediction process, a quantile regression layer is embedded within the BiGRU network to obtain the predicted capacity at the 0.5 quantiles. By conducting a comparative analysis with other prediction methods using the publicly available NASA and CALCE datasets, the results demonstrate that the proposed model further enhances the accuracy of lithium-ion battery RUL prediction. The main contributions and innovations of this study are as follows:

(1) By employing autoencoders for denoising distorted data, the issue of increased prediction error caused by data distortion is effectively mitigated.

(2) The model extracts deep representative features hidden in the original measurement signals using 1D-CNN and subsequently estimates battery capacity with BiGRU. This approach addresses the computational challenges and burdens associated with using a single GRU model when handling large volumes of data.

(3) This method accounts for the phenomenon of capacity regeneration by embedding a quantile regression (QR) layer into the BiGRU network. By constructing a quantile regression loss function, it characterizes and quantifies the uncertainty caused by capacity regeneration.

(4) Comparative analysis with several advanced methods on publicly available battery aging datasets demonstrates the effectiveness and superiority of the proposed approach.

The remainder of this paper is organized as follows: Section 2 provides a detailed description of the model and methods. Section 3 presents the research results, and Section 4 concludes the paper.

2. Methods for Predicting RUL of Lithium-Ion Batteries

The comprehensive RUL prediction method for lithium-ion batteries proposed in this study is illustrated in Fig 1 The model addresses the uncertainty in predicting the lifespan of lithium-ion batteries under different operating conditions and the noise present in the data collection process. It proposes a quantile regression-based prediction method utilizing a DAE-CNN-BiGRU.

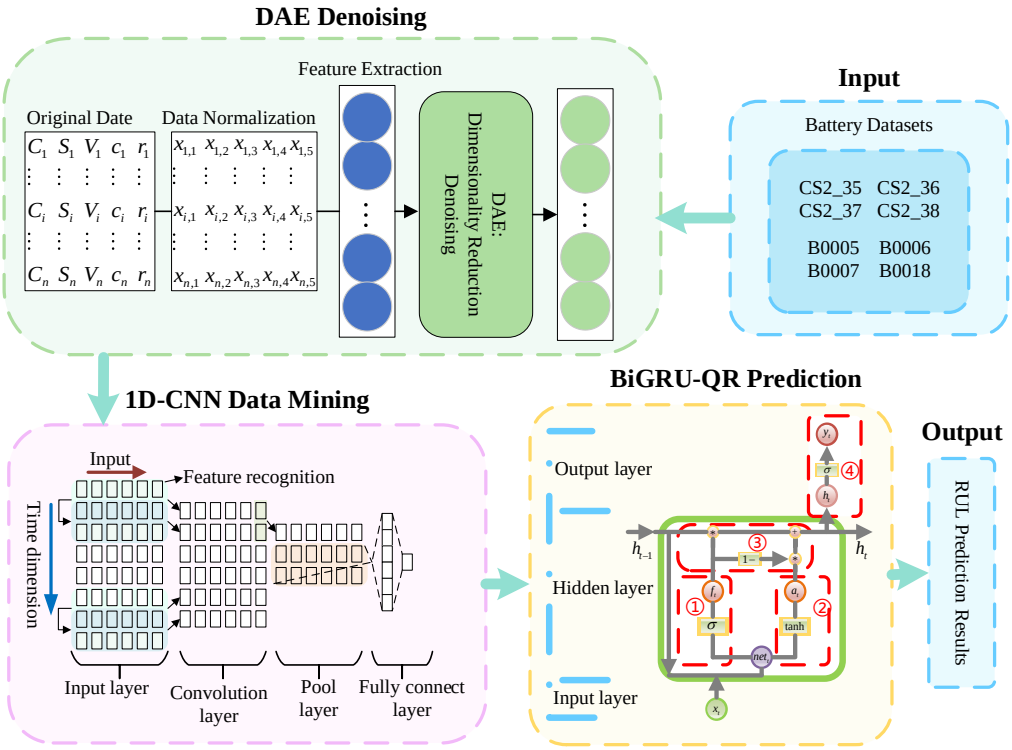

Fig 1 Basic framework of the RUL prediction model for lithium-ion batteries.

The specific procedural steps are as follows:

Step 1: First, extract the battery degradation feature dataset from the operational data. Then, use an autoencoder to denoise the distorted data, addressing the issue of increased prediction errors caused by data distortion. Afterward, the dataset is divided into training and testing sets, completing the data preprocessing stage.

Step 2: Utilize a 1D-CNN, consisting of convolutional layers, pooling layers, nonlinear layers, and fully connected layers, to extract deep representative features hidden in the original measurement signals.

Step 3: Integrate the quantile regression (QR) layer into the BiGRU network. By constructing a quantile regression loss function, the model characterizes and quantifies the uncertainty caused by capacity regeneration, enabling accurate estimation of battery capacity using the BiGRU model.

Step 4: Evaluate and compare the predictive performance of various data-driven models to obtain the final prediction results.

2.1 Denoising Autoencoder (DAE)

In the model, considering that noise in the data can significantly impact the prediction accuracy of the neural network, a denoising autoencoder is employed to preprocess the data and minimize the influence of noise before feeding it into the neural network. In this paper, the DAE algorithm is employed to address the issue of noise interference, thereby reducing the loss of critical information and improving the prediction performance of the CNN-BiGRU-QR model, as shown in Fig 2.

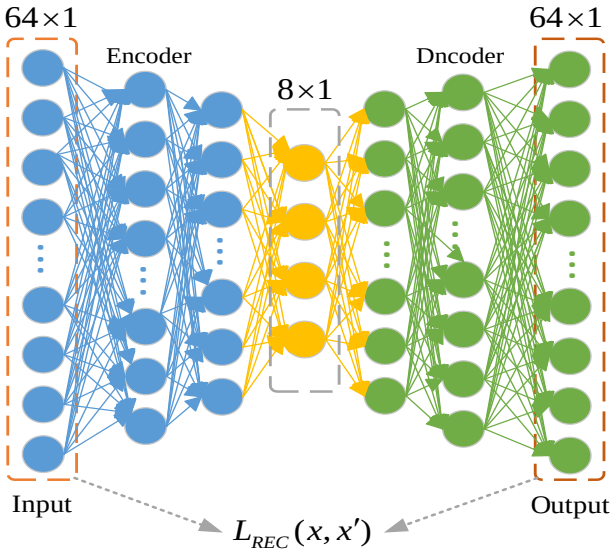

Fig 2 The structure of the DAE in lithium-ion battery prediction.

The encoder of the DAE divides the input raw aging data sequence x_t into m sequence samples, Denoted as $x_t = \{x_{t+1}, x_{t+2}, \cdots x_{t+m}\}$. Incorporating Gaussian white noise into the raw data series of lithium-ion batteries can enhance the model's nonlinear expressiveness and robustness, enabling the generation of new input data.y_t. The compressed data from the encoder is expressed as shown in Equation (1), while the reconstructed output data from the decoder is given in Equation (2).

$$z = \sigma(W_1 y_t + b) \tag{1}$$

$$x_t' = f'(W_2 z + b') \tag{2}$$

where b、$\sigma(.)$、z represent the bias, activation function, and output of the DAE encoder; $W_1 = W_2^T = W$ are the weight matrices for encoding and decoding; Additionally, b'、f' denote the bias and the mapping of the DAE encoder's output layer. To enhance the sparsity of the network, mitigate overfitting, and reduce computational complexity, the ReLU function is selected as the activation function for the hidden layers in both the encoder and decoder. Since the Sigmoid function can map the network's output values to the range of (0, 1), it is chosen as the activation function for the output layer to effectively map the output data within a valid range. Thus, the loss function for the DAE component is defined as:

$$L_d = L_{MSE} + L_{REC} = \frac{1}{n}\sum_{t=1}^{n} l(y_t - x_t) + \lambda\left(\|W\|_F^2 + \|W'\|_F^2\right) \tag{3}$$

where L_{MSE} represents the mean squared error loss function, $l(.)$ denotes the reconstruction error loss function and λ is the weight parameter. The structure of the DAE is symmetric, allowing the weights at corresponding symmetric positions to be equal. This reduces the number of weights in the model and accelerates the training process.

The lithium-ion battery data involved in this study is complex, encompassing various time-varying monitoring indicators such as voltage, current, and temperature. From a theoretical perspective, based on the principles of signal sampling and information retention in information theory, for such complex time-series data, there exists an optimal dimensional range that balances information integrity and computational complexity. In this paper, by training the DAE, the high-dimensional vectors are split into multiple 64-dimensional input vectors as the input to the DAE, with the corresponding raw data similarly divided to serve as the labels for the DAE. The encoding part of the encoder compresses the 64-dimensional vector into an 8-dimensional vector, while the decoding part expands the compressed vector back to 64 dimensions, facilitating the learning of noise characteristics. Additionally, to mitigate the impact of variations in data distribution on the neural network, the denoised data is subjected to normalization.

2.2 Convolutional Neural Network(1D-CNN)

The one-dimensional convolutional neural network (1D-CNN) model employed in this study primarily consists of convolutional layers, pooling layers, nonlinear activation layers, and fully connected layers, as illustrated in Fig 3.

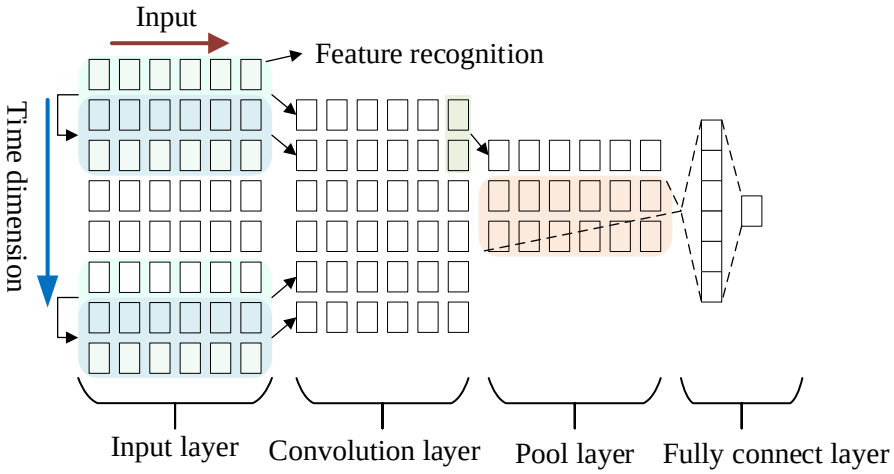

Fig 3 Architecture of the One-Dimensional CNN

The convolutional layer performs convolution operations on the preprocessed data through convolutional filters, extracting features and generating the corresponding feature maps. The pooling layer performs sampling while retaining the primary information of the feature vectors, primarily serving to deeply extract internal data features and achieve dimensionality reduction. The nonlinear layer, also known as the activation function layer, introduces nonlinear elements into the constructed model. The fully connected layer is primarily used to integrate the extracted features and pass them through the activation function, further refining the model structure. The specific mathematical formula is as follows:

$$Y_{conv}^{m+1} = \varphi(W * X + b) \tag{4}$$

Where X represents the input sequence; φ is the nonlinear activation function; W denotes the weights; b is the bias term; and Y is the output of the feature extraction result. The output after the pooling operation is given by the following formula:

$$Y_{pool}^{m+1} = Pooling(Y_{pool}^{m+1}) \tag{5}$$

In this study, the 1D-CNN model consists of two layers: one convolutional layer and one pooling layer. The convolutional kernels in the convolutional layer are capable of adaptively extracting the local spatial features of the signal. Furthermore, the convolution operation employs the ReLU activation function, which, compared to the traditional sigmoid activation function, better addresses the issues of gradient explosion and vanishing gradients, as it does not suffer from non-differentiable points. The pooling layer utilizes a max pooling operation to reduce the feature dimensions while preserving the primary feature information in the signal.

2.3 Bidirectional Gated Quantile Neural Network (BiGRU-QR)

The gated recurrent unit (GRU) [25] is a variant of the long short-term memory (LSTM) network, both of which belong to the family of recurrent neural networks (RNNs). Compared to LSTM, GRU introduces structural optimizations by integrating a reset gate and an update gate, which enhance training efficiency while preserving memory capability. GRU not only retains the advantages of LSTM but also features a more compact structure, fewer parameters, and improved convergence properties, leading to reduced training time and enhanced predictive

efficiency. As illustrated in Fig 4(a), the network architecture of GRU is shown. The operations of GRU at each time step are governed by the previous output h_{t-1} and the current input x_t. The equations for computing GRU at a given time step are as follows:

$$r_t = \sigma(W_r x_t + U_r h_{t-1} + b_r) \tag{6}$$

$$z_t = \sigma(W_z x_t + U_z h_{t-1} + b_z \tag{7}$$

$$\tilde{h}_t = \tanh\left(W_{\tilde{h}} x_t + U_{\tilde{h}}\left(r_t \odot h_{t-1}\right) + b_{\tilde{h}}\right) \tag{8}$$

$$h_t = \left(1 - z_t\right) \odot h_{t-1} + z_t \odot \tilde{h}_t \tag{9}$$

where σ and tanh represent the Sigmoid and tanh activation functions, respectively. r_t and z_t correspond to the reset gate and update gate, while $\tilde{h}_t$ denotes the process vector between the current input t and the hidden state h_{t-1} from the previous time step. x_t represents the input at the current time step. W and U are the neuron weight matrices, and b denotes the bias term. The update gate z_t dynamically regulates $\tilde{h}_t$ and h_{t-1}, determining the final output h_t.

BiGRU is an improved variant of GRU that incorporates both forward and backward contextual information, achieving higher accuracy in time series prediction compared to the unidirectional GRU. As illustrated in Fig 4(b), the BiGRU architecture consists of a forward GRU layer and a backward GRU layer. The horizontal axis represents the bidirectional flow of time series data, while the vertical axis denotes the unidirectional propagation of information from the input layer to the hidden layer and subsequently to the output layer. The final output is computed using the following equations:

$$h_t = \left[\vec{h}_t \oplus \overleftarrow{h}_t\right] = concat\left(\vec{h}_t, \overleftarrow{h}_t\right) \tag{10}$$

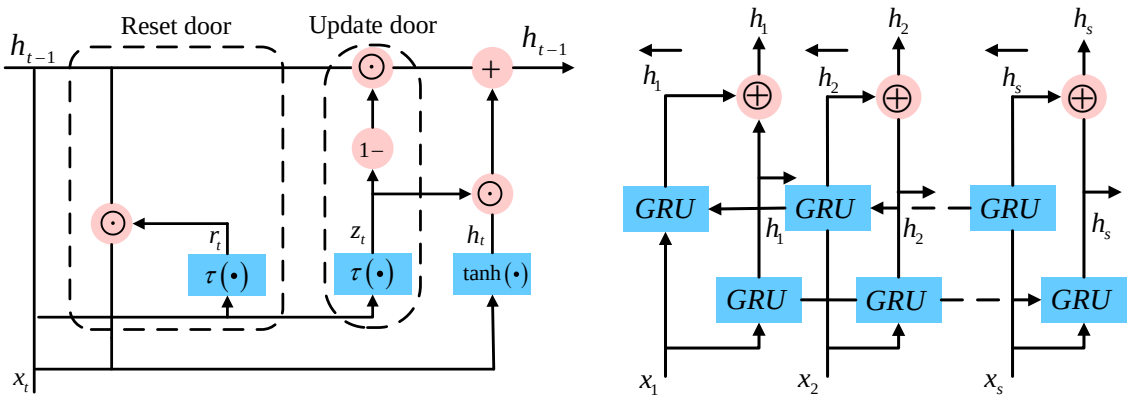

(a) GRU (b) BiGRU

Fig 4 Unit Structures of GRU and BiGRU

Quantile Regression (QR), introduced by Koenker et al., is a regression model that employs data at various quantiles for analysis [26]. This approach offers a more comprehensive view of the relationships between variables by examining different quantile levels. Traditional regression analysis is limited to capturing only the central tendency of the dependent variable, without providing insights into the overall distribution. In contrast, the Quantile Regression (QR) model addresses this limitation by allowing an examination of how explanatory variables influence different aspects of the distribution.

Additionally, a hybrid model integrating quantile regression with a bidirectional gated recurrent unit (BiGRU) is proposed to quantify predictive uncertainty, referred to as BiGRU-QR, as illustrated in Fig 5.

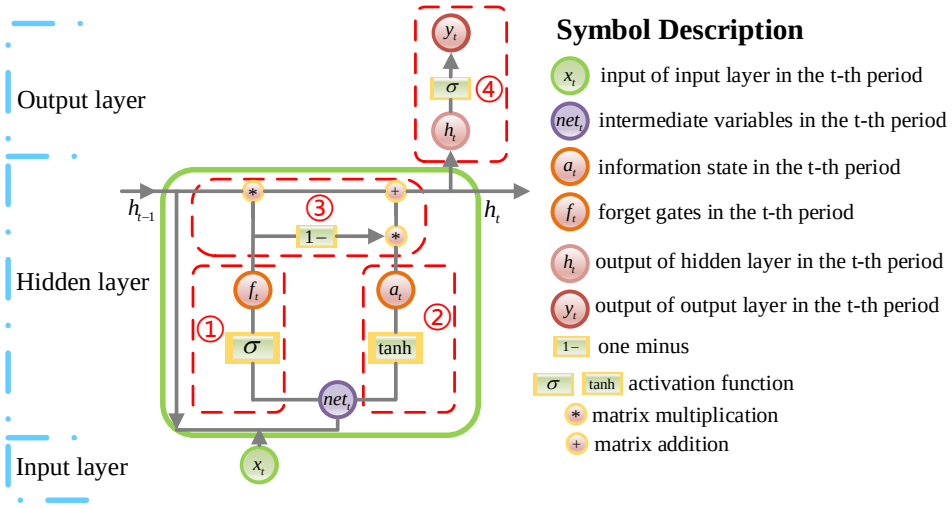

Fig 5 Schematic Representation of the BiGRU-QR Network Architecture

The core of BiGRU-QR lies in the computation of $f\left(x_t,\Omega(\tau)\right)$. The computational steps of BiGRU-QR are as follows:

①Compute the forget gate $f_t(\tau)$ and the coupled output gate $i_t(\tau)$

$$f_t(\tau)=\sigma\left(net_t(\tau)\right)=\sigma\left(\omega_h(\tau)\cdot h_{t-1}(\tau)+\omega_x(\tau)\cdot x_t\right) \tag{11}$$

$$i_t(\tau)=1-f_t(\tau) \tag{12}$$

②Compute the information state at time step t

$$a_t(\tau)=\tanh\left(net_t(\tau)\right)=\tanh\left(\omega_h(\tau)\cdot h_{t-1}(\tau)+\omega_x(\tau)\cdot x_\tau\right) \tag{13}$$

③Compute the output of the hidden layer h_t

$$h_t(\tau)=f_t(\tau)*h_{t-1}(\tau)+i_t(\tau)*a_t(\tau) \tag{14}$$

④Compute $f\left(x_t,\Omega(\tau)\right)$

$$Q_{y_t}(\tau/x_t)=f\left(x_t,\Omega(\tau)\right)=\sigma\left(z_t(t)\right)=\sigma\left(\omega_y(\tau)\cdot h_t(\tau)\right) \tag{15}$$

BiGRU-QR retains the original network architecture and functionality of BiGRU while incorporating nonlinear quantile regression through an optimized objective function, enabling more accurate time series prediction based on historical data. Additionally, quantile regression estimates prediction intervals by regressing on specific quantiles of the forecasted values. In the model, the objective function for quantile regression is employed, and the optimal parameter estimates are obtained by minimizing this objective function. The quantile regression loss function is defined as follows:

$$\min_{W(\tau),U(\tau)}\frac{1}{T}\sum_{i=1}^{T}\left\{\rho_\tau\left[y_i-\hat{Q}_{y_i}(\tau)\right]\right\}=\frac{1}{T}\sum_{i=1}^{T}\left\{\left\{\tau-I\left[y_i-\hat{Q}_{y_i}(\tau)\right]\right\}\left[y_i-\hat{Q}_{y_i}(\tau)\right]\right\} \tag{16}$$

where T denotes the length of the predicted output, τ represents the quantile probability,y_i is the actual value of the sample, and $\hat{Q}_y(\tau)=\mathrm{g}\left(X,W(\tau),U(\tau)\right)$ is the output of the Bi-GRU under the quantile condition.

The exponential function I(u) is defined as:

$$I(u)=\begin{cases}0 & u>=0\\ 1 & u<0\end{cases} \tag{17}$$

Where, $u = y_i - \hat{Q}_{y_i}$

When τ>0.5, quantile regression emphasizes the upper portion of the data distribution, leading to predictions that tend to estimate higher battery capacity values. Conversely, when τ<0.5, the regression focuses on the lower portion of the distribution, resulting in predictions biased toward lower capacity estimates. When τ=0.5, quantile regression directly estimates the median of the predicted battery capacity, which serves as a robust representative value, effectively mitigating the influence of outliers. Therefore, in this study, selecting τ=0.5 for battery capacity prediction allows for better handling of anomalies in asymmetrically distributed data, providing a more representative and reliable estimate.

In this work, a quantile regression layer is embedded prior to the output layer of the BiGRU network, enabling the model to generate prediction intervals alongside point forecasts. This enhancement significantly improves the model's capability to express the uncertainty associated with future capacity trends. The proposed BiGRU-QR model integrates the strengths of bidirectional gated recurrent units with quantile regression, thereby achieving effective uncertainty quantification in lithium-ion battery capacity forecasting. By capturing complex patterns and latent dependencies within the battery data, the BiGRU-QR model not only delivers accurate capacity predictions but also provides reliable and comprehensive uncertainty estimates. This dual capability offers valuable support for the prediction of the remaining useful life of lithium-ion batteries.

3. Model Validation and Evaluation

3.1 Dataset Information

To validate the accuracy of the proposed method, this study employs two publicly available battery datasets for the prediction of lithium-ion battery's remaining useful life (RUL). The first dataset is provided by the NASA Research Center, while the second originates from the Center for Advanced Life Cycle Engineering (CALCE) at the University of Maryland. The experimental operating parameters of the batteries are summarized in

Table 1.

The NASA dataset consists of four lithium-ion batteries, labeled B0005, B0006, B0007, and B0018, each with a rated capacity of 2Ah. During charging, the batteries undergo constant current (CC) charging at a controlled current of 1.5A. Once the terminal voltage reaches 4.2V, charging transitions to a constant voltage (CV) mode at 4.2V until the current decreases to 20mA. The discharge tests are conducted at a constant current of 2A until the voltage reaches a predefined cutoff threshold.

In this study, the CALCE dataset from the CS battery series is utilized, including batteries CS2_35, CS2_36, CS2_37, and CS2_38, each with a rated capacity of 1.1Ah. The battery data from the CALCE Research Center follow a standardized constant current – constant voltage (CC-CV) charging protocol. During constant current charging, the charging current is maintained at 0.5A until the terminal voltage reaches 4.2V, after which constant voltage charging is applied until the current decreases below 0.05A.

Table 1 Battery Experimental Dataset Information

Battery	Battery Experimental Conditions				
	Charing cut-off voltage (V)	Discharging cut-off voltage (V)	Charge current (A)	Discharge current (A)	temperature (℃)
B0005	4.2	2.7	1.5	2	24
B0006	4.2	2.5	1.5	2	24

B0007	4.2	2.2	1.5	2	24
B0008	4.2	2.5	1.5	2	24
CS2_35	4.2	2.7	0.5	1	24
CS2_36	4.2	2.7	0.5	1	24
CS2_37	4.2	2.7	0.5	1	24
CS2_38	4.2	2.7	0.5	1	24

Continuous charge-discharge cycling experiments were conducted on the batteries, with failure defined as the point where the battery capacity declines to 70% of its rated value. Accordingly, in the NASA dataset, the failure threshold is set at 1.4Ah, while in the CALCE dataset, the threshold is set at 0.77Ah. The capacity degradation curves for both datasets are shown in Fig 6.

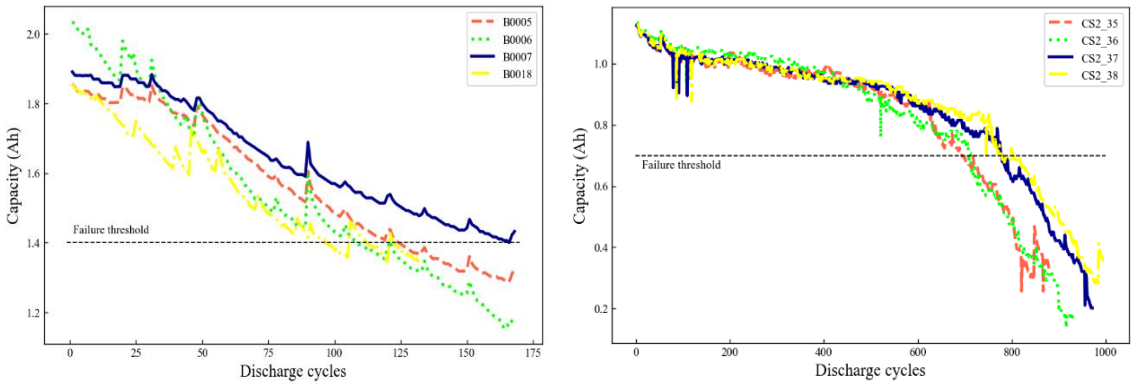

（a）NASA dataset　　（b）CALCE dataset

Fig 6 Capacity Degradation Curves of Lithium-Ion Batteries.

As illustrated in the figure, the battery capacity degradation exhibits a non-monotonic downward trend with increasing cycle numbers. An in-depth analysis of the data distribution characteristics in the NASA and CALCE datasets reveals that the capacity data in both datasets follow an asymmetric distribution. Taking the NASA dataset as an example, during the battery degradation process, the early stage is characterized by a relatively slow decline in capacity, with data points densely concentrated. In contrast, as battery aging progresses in the later stages, the degradation rate accelerates and the data becomes increasingly dispersed. This distribution pattern reflects the varying performance characteristics of batteries at different aging stages.

In terms of inter-cell variability, despite having the same initial rated capacity, batteries B0005, B0006, B0007, and B0018 in the NASA dataset demonstrate distinct differences in the onset of degradation, degradation rate, and fluctuation patterns—largely due to factors such as manufacturing variability. Similar discrepancies are also observed among batteries CS2_35, CS2_36, CS2_37, and CS2_38 in the CALCE dataset. These differences inevitably influence model training. Nevertheless, the proposed model in this study is capable of learning and adapting to such variations, achieving robust prediction performance across different battery instances. This demonstrates the model's strong adaptability and further substantiates the reliability of the experimental results.

3.2 DAE Denoising Analysis

During the battery energy regeneration phase, the internal chemical reactions are complex and unstable, leading to abnormal fluctuations in signals such as voltage and current. The instantaneous current surges generated during the energy regeneration process may overlap with inherent noise present during data collection, causing the measured data to deviate from the true values. Such deviations can interfere with the accurate assessment of the battery's actual state, subsequently affecting the feature extraction and model training processes.

To validate the feasibility and effectiveness of the DAE denoising method, denoising capability experiments were conducted. Initially, Gaussian noise is introduced into the voltage signals of four battery cells. Subsequently,

denoising methods such as EMD, EEMD, and DAE are applied to the noisy signals. Finally, the signal-to-noise ratio (SNR) of the processed signals is calculated. The Signal-to-Noise Ratio (SNR) is the ratio of signal energy to noise energy and is commonly used in signal detection fields. A higher SNR indicates less noise in the signal. The denoising results from the three methods are shown in Table 2.

Table 2. SNR of Three Denoising Methods Post-Denoising (dB).

Method	B0005	B0006	B0007	B0018
DAE	37.19	31.27	35.48	32.67
EEMD	17.11	16.58	20.79	20.19
EMD	4.75	10.95	9.56	17.11

Therefore, to address the issue of noise interference, this study employs a DAE to denoise the battery dataset, thereby reducing the loss of critical information. The denoising results are illustrated in Fig 7.

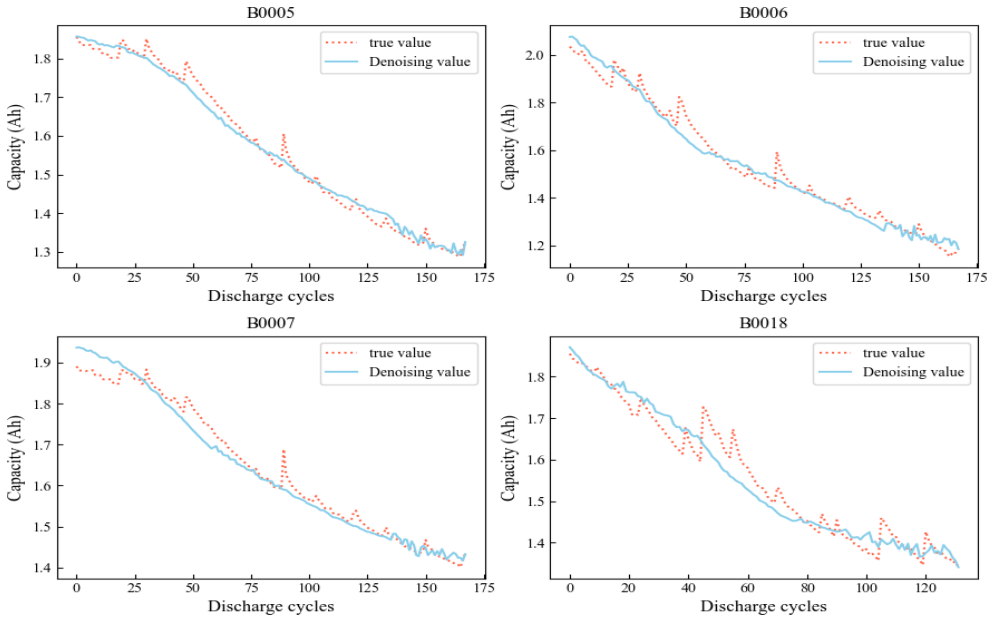

Fig 7 DAE Denoising Effect Illustration.

The comparison between the capacity variation trends after DAE denoising and the laboratory-measured capacity variation trends reveals that the capacity variation curves after DAE denoising are smoother. This indicates that DAE effectively reduces fluctuations and noise in the data. Additionally, by learning the data distribution and key characteristics of the signals, the DAE maintains a similar overall decline trend and variation pattern as the actual measurements after denoising. This ensures that crucial signal features are accurately reconstructed, preserving the signal's energy.

3.3 Effectiveness Analysis of the Model

To validate the effectiveness of the method proposed in this study, the CALCE lithium battery dataset was divided into two parts: 70% of the dataset was designated as the training set, utilized to train the model through iterative learning processes, and the remaining 30% was allocated as the test set. The test set served to evaluate whether the training process met established standards and to assess the overall performance of the model. Compared to the CALCE dataset, the NASA dataset contains only approximately 170 charge-discharge cycles. Therefore, 50% of the NASA dataset was utilized for model training, while the remaining data were used to estimate the battery's remaining useful life (RUL). Furthermore, a comparative analysis was conducted against nine commonly used models: MLP, CNN, RNN, LSTM, GRU, BiGRU, BiLSTM, CNN-BiGRU, and CNN-BiLSTM.

3.3.1 Capacity Degradation Curves

In the capacity degradation curves, the LSTM, GRU, Bi-GRU, Bi-LSTM, CNN-Bi-GRU, and CNN-Bi-LSTM models are selected for training and testing on the four publicly available lithium-ion battery datasets from NASA and CALCE. The predicted capacity from the proposed method is compared with the results from these models. The comparison of capacity degradation curves is illustrated in Fig 8 andFig 9.

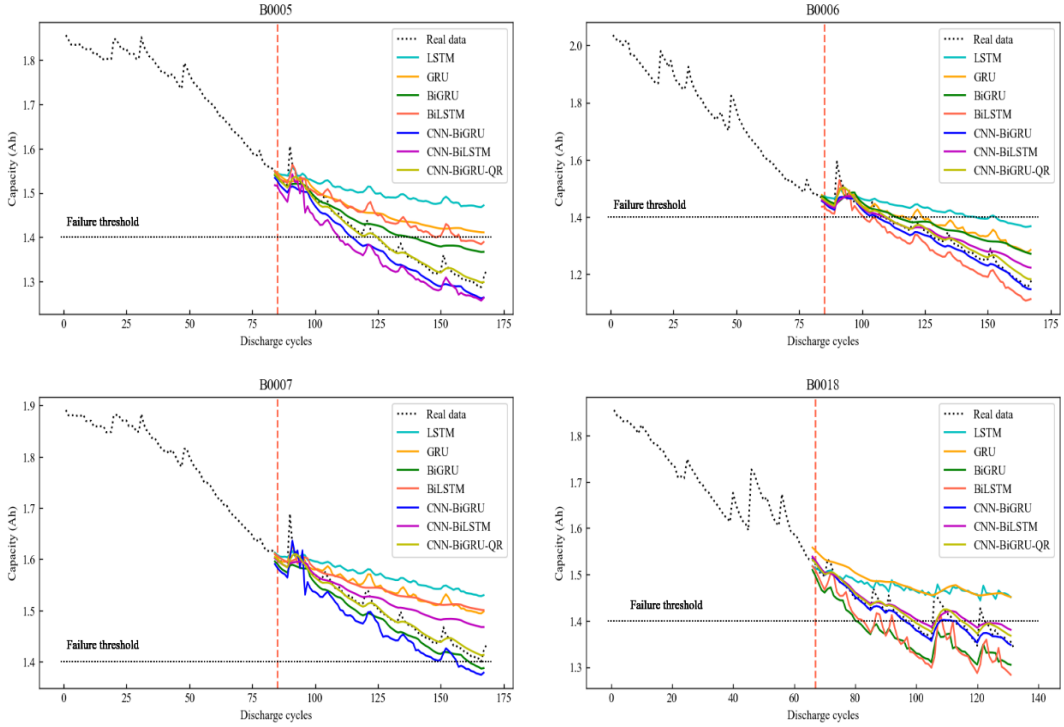

Fig 8 Comparison of NASA Capacity Degradation Curves

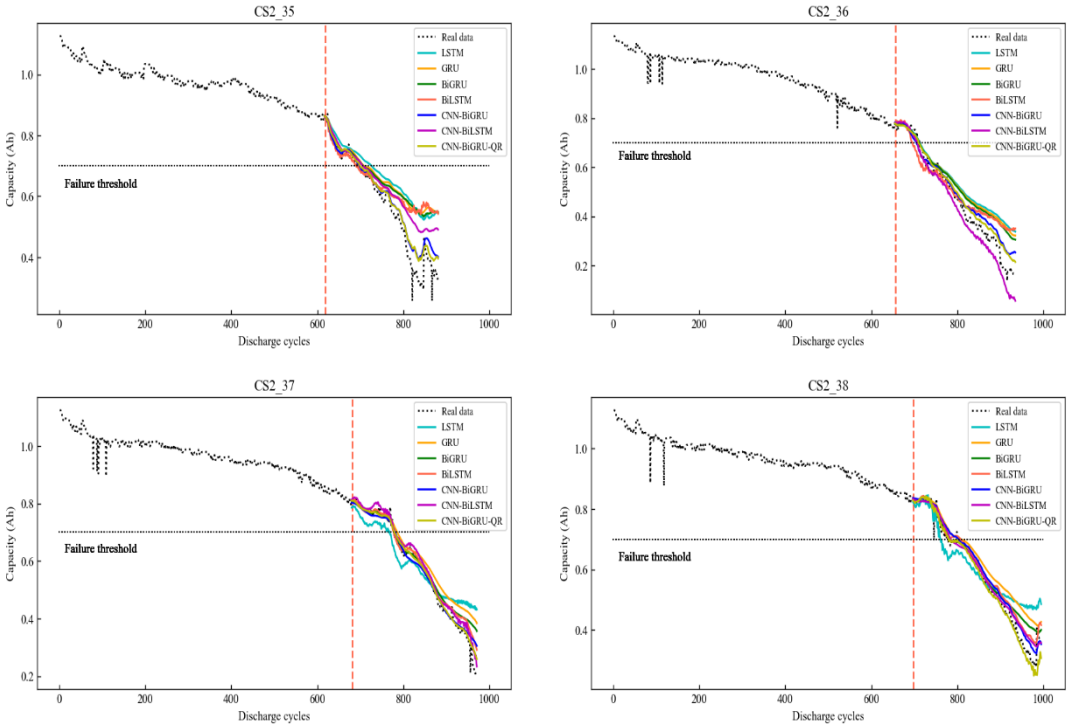

Fig 9 Comparison of CALCE Capacity Degradation Curves

In the NASA dataset degradation curves, it can be observed that the LSTM model generally tends to overestimate the remaining capacity during higher cycle counts (e.g., after 100 cycles), indicating a bias towards

predicting better capacity retention. The GRU model exhibits similar behavior to LSTM, but in certain cases (such as B0007 and B0018), its predictions deviate more significantly from the actual data, particularly at later cycles. Models that combine CNN with BiGRU and BiLSTM, such as CNN-BiGRU and CNN-BiLSTM, typically capture the capacity degradation trend more effectively, especially in B0005 and B0006, where the predicted results closely align with the actual data. The CNN-BiGRU-QR model performs relatively better, particularly in predicting capacity at higher cycle counts, with its curves closely tracking the actual data. This demonstrates the proposed model's advantages in handling temporal and complex features. Similarly, in the CALCE dataset degradation curves, the proposed model also demonstrates high accuracy.

The effectiveness of the proposed model can be visually demonstrated through a comparison of residual box plots from various models, as shown in Fig 10 Fig 11.

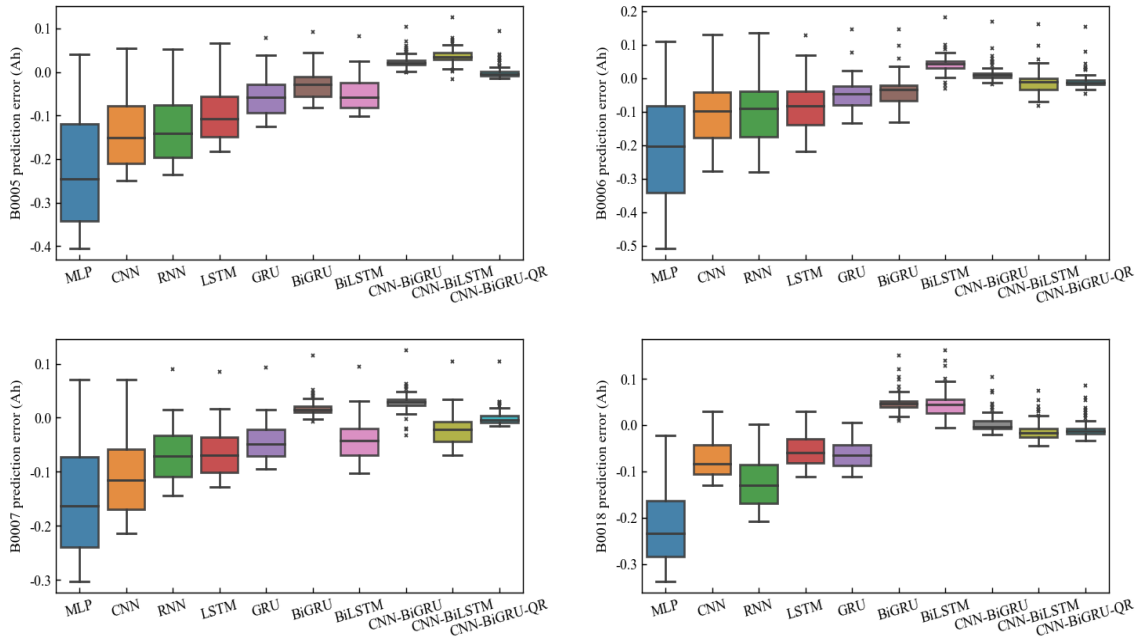

Fig 10 NASA Residual Box Plot

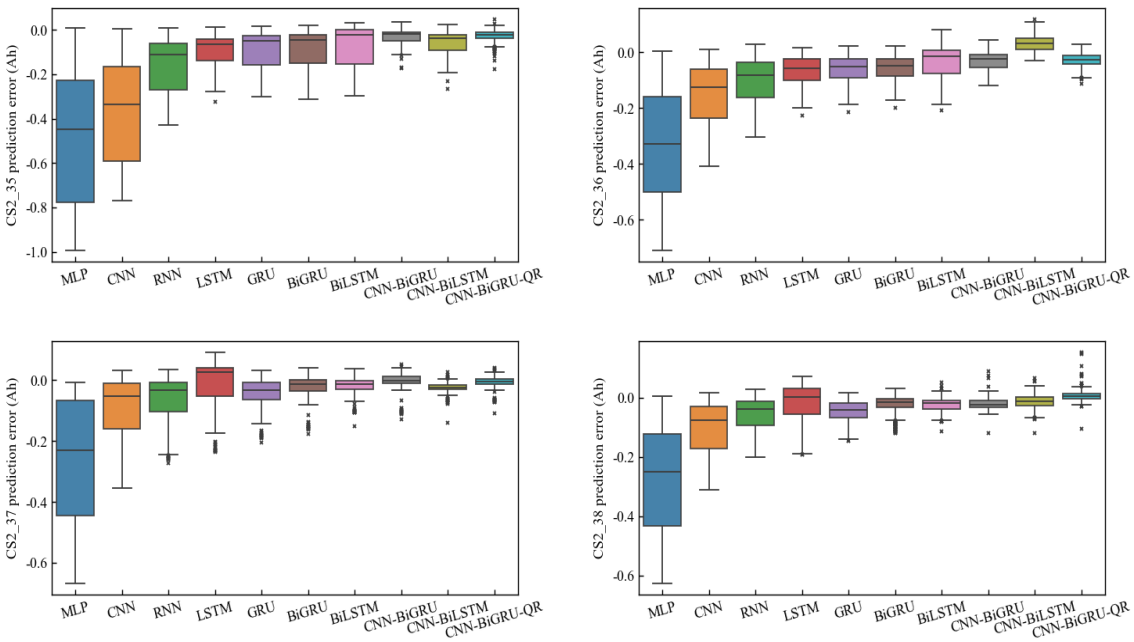

Fig 11 CALCE Residual Box Plot

Taking the B0005 battery as an example for comparative analysis, it can be observed that:

(1) Residual Distribution of Different Models:

The Fig presents the residual distributions of various models (such as MLP, CNN, RNN, LSTM, GRU, etc.). By comparing the box plots of each model, we can observe the error performance across different models in their predictions.

(2) Central Tendency and Dispersion of Residuals:

Central Tendency: The position of the median line within each box plot represents the median of the residuals. Most models have medians close to 0, but some models (such as MLP and GRU) show significant deviations from 0.

Dispersion: The height of the box and the length of the whiskers represent the degree of residual dispersion. Shorter boxes and whiskers indicate more concentrated residuals. It can be seen that the residual distributions of the CNN-BiLSTM and CNN-BiGRU-QR models are more concentrated, with less fluctuation.

(3) Outliers and Anomalies: In the Fig, several box plots exhibit numerous outliers beyond the whiskers (marked by small black dots), as seen in models like BiGRU, BiLSTM, and CNN-BiGRU. These outliers indicate that these models produced significant errors in certain predictions.

Based on this information, a more comprehensive evaluation of the predictive performance of different models can be made. For example, the MLP model exhibits a wide residual distribution range with a notable negative bias, indicating larger errors and relatively poor predictive performance. In comparison, the CNN and RNN models show a narrower residual distribution, demonstrating an improvement in prediction accuracy over MLP. The combination models, such as CNN-BiGRU and CNN-BiLSTM, exhibit the most concentrated residual distributions, with fewer outliers, suggesting they provide the best predictive performance. Additionally, the median of the residuals reveals whether there is systematic bias in the models. Most models have medians close to 0, indicating no significant systematic bias overall. However, some models, such as MLP, show a clear negative bias.

3.3.2 Model Evaluation

In regression problems, the four most commonly used and reliable evaluation metrics for assessing the predictive accuracy of different models are Root Mean Square Error (RMSE), Mean Absolute Error (MAE), Mean Absolute Percentage Error (MAPE), and the coefficient of determination (R^2). These metrics are employed to analyze the discrepancies between the true values and predicted values of lithium-ion battery's remaining lifespan. Table 3 andTable 4 present the experimental results for the four metrics: RMSE, MAE, MAPE, and R^2. Fig 12 andFig 13 illustrates a comparative analysis of these evaluation metrics.

Table 3 NASA Model Evaluation Results

Method	B0005				B0006			
	RMSE	MAE	MAPE	R^2	RMSE	MAE	MAPE	R^2
LSTM	0.1142	0.1012	7.4459	-1.0255	0.1113	0.0948	7.4327	-0.2622
GRU	0.0712	0.0616	4.5406	0.2124	0.0669	0.0555	4.3406	0.5437
BiGRU	0.0433	0.0356	2.6284	0.7089	0.0602	0.0494	3.8480	0.6305
BiLSTM	0.0627	0.0552	4.0577	0.3897	0.0490	0.0431	3.2580	0.7552
CNN-BiGRU	0.0290	0.0244	1.7519	0.8688	0.0280	0.0161	1.1692	0.9199
CNN-BiLSTM	0.0417	0.0381	2.7240	0.7296	0.0380	0.0272	2.1001	0.8529
CNN-BiGRU-QR	0.0157	0.0097	0.6907	0.9615	0.0273	0.0192	1.4458	0.9239

Method	B0007				B0018			
	RMSE	MAE	MAPE	R^2	RMSE	MAE	MAPE	R^2
LSTM	0.0773	0.0682	4.6414	-0.4287	0.0647	0.0558	4.0095	-0.7665
GRU	0.0555	0.0478	3.2591	0.2639	0.0687	0.0628	4.4896	-0.9877
BiGRU	0.0234	0.0183	1.2144	0.8682	0.0542	0.0495	3.49238	-0.2376

BiLSTM	0.0544	0.0461	3.1453	0.2921	0.0546	0.0452	3.20716	-0.2562
CNN-BiGRU	0.0347	0.0314	2.0906	0.7107	0.0231	0.0136	0.9461	0.7750
CNN-BiLSTM	0.0349	0.0278	1.8956	0.7081	0.0250	0.0217	1.5442	0.7349
CNN-BiGRU-QR	0.0153	0.0091	0.6035	0.9436	0.0228	0.0188	1.3298	0.7794

Table 4 CALCE Model Evaluation Results

Method	CS2_35				CS2_36			
	RMSE	MAE	MAPE	R^2	RMSE	MAE	MAPE	R^2
LSTM	0.1177	0.0937	22.2400	0.4728	0.0717	0.0913	25.8666	0.7732
GRU	0.1147	0.0852	21.0529	0.4994	0.0841	0.0658	23.7860	0.8077
BiGRU	0.1128	0.0814	20.3980	0.5157	0.0769	0.0606	21.7475	0.8392
BiLSTM	0.1104	0.0727	19.0375	0.5362	0.0774	0.0553	21.0881	0.8372
CNN-BiGRU	0.04248	0.0309	7.6312	0.9313	0.0445	0.0354	12.3722	0.9461
CNN-BiLSTM	0.0847	0.0630	15.4722	0.7267	0.0453	0.0368	12.2382	0.9440
CNN-BiGRU-QR	0.0393	0.0292	7.0077	0.9412	0.0375	0.0306	10.2185	0.9618

Method	CS2_37				CS2_38			
	RMSE	MAE	MAPE	R^2	RMSE	MAE	MAPE	R^2
LSTM	0.0722	0.0551	13.9511	0.8303	0.0722	0.0526	12.6228	0.8204
GRU	0.0596	0.0425	11.5802	0.8844	0.0622	0.0485	11.3704	0.8671
BiGRU	0.0426	0.0265	7.7324	0.9408	0.0420	0.0276	6.9620	0.9393
BiLSTM	0.0323	0.0216	6.0333	0.9659	0.0332	0.0258	6.0503	0.9620
CNN-BiGRU	0.0273	0.0168	4.4349	0.9758	0.0285	0.0234	4.9810	0.9721
CNN-BiLSTM	0.0281	0.0239	5.4921	0.9743	0.0279	0.0203	4.6898	0.9732
CNN-BiGRU-QR	0.0196	0.0131	3.2647	0.9875	0.0244	0.0141	3.0686	0.9795

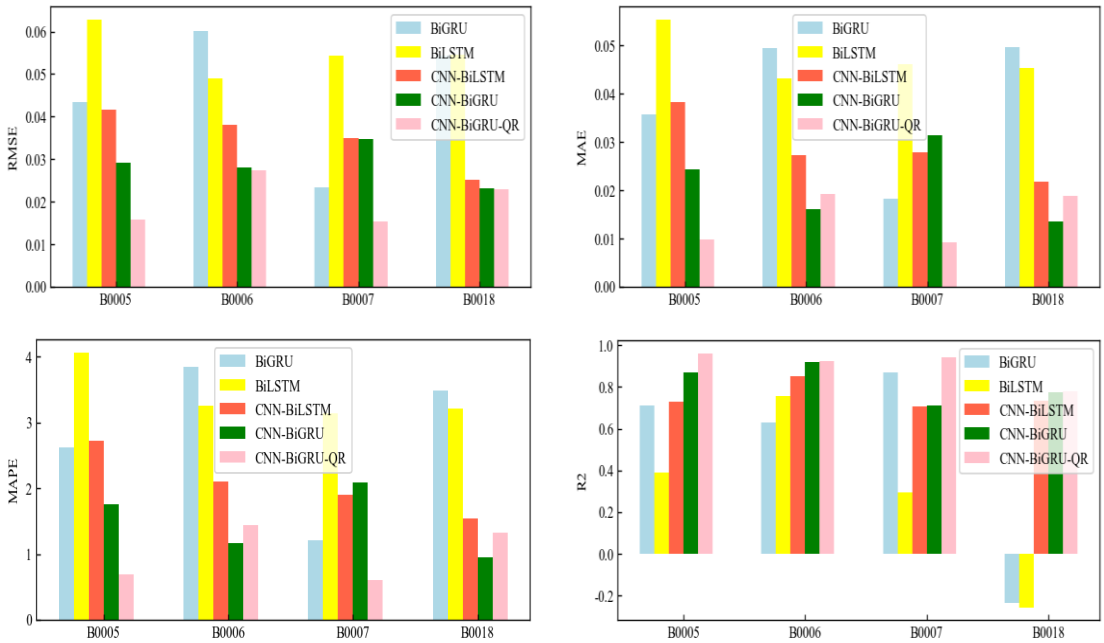

Fig 12 Comparison of NASA Evaluation Metrics

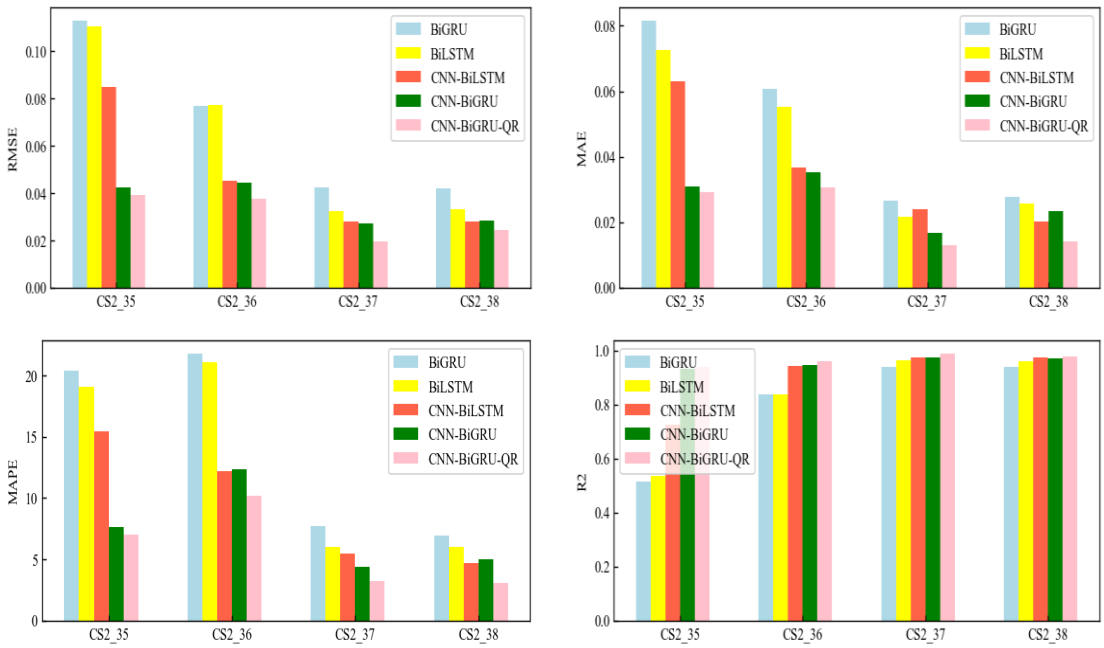

Fig 13 Comparison of CALCE Evaluation Metrics

Based on Tables 3 and 4, as well as Fig 12 andFig 13, the experimental results of different models on the NASA and CALCE datasets can be analyzed. The BiGRU and BiLSTM models exhibit relatively poor performance across various metrics, particularly in terms of RMSE, MAE, and MAPE. In contrast, the CNN-BiGRU-QR model demonstrates the best performance across all datasets. Specifically, for the NASA battery datasets B0005, B0006, B0007, and B0018, the proposed method achieves RMSE values of 1.57%, 2.73%, 1.53%, and 2.28%, respectively, and MAE values of 0.97%, 1.92%, 0.91%, and 1.88%. The estimated RMSE and MAE obtained by the proposed method are consistently lower than those of other approaches, indicating not only its accurate prediction capability but also its distinct advantages.Regarding the evaluation results on the CALCE dataset, the CNN-BiGRU-QR model outperforms the other nine models in all evaluation metrics (RMSE, MAE, MAPE, and R^2) across all battery datasets. This highlights its superior accuracy and generalization ability in the task of battery RUL prediction, thereby validating the effectiveness of the proposed CNN-BiGRU-QR model. Furthermore, for the four NASA battery datasets, the corresponding correlation coefficients (R^2) are 0.9615, 0.9239, 0.9436, and 0.7794, respectively. While the proposed method does not achieve a significant improvement in prediction accuracy for battery B0018, it still yields satisfactory results, demonstrating its optimal predictive precision and fitting performance.

Moreover, based on the experimental data, using the NASA B0005 battery from the dataset as an example, during the early stage of battery capacity degradation, the error between the predicted and actual values of the BiGRU-QR model is relatively small, with the residuals concentrated. This is because the BiGRU model effectively learns the relatively stable capacity change patterns of the battery during this phase, and the quantile regression layer quantifies uncertainty based on these stable features, resulting in more reliable prediction intervals. As the cycle number increases, the internal chemical reactions of the battery become more complex, and capacity fluctuations emerge. In this stage, the bidirectional structure of the BiGRU model comes into play, and by combining it with the quantile regression layer, the model continues to closely track the capacity change trends with minimal residual fluctuation. In comparison with other models, such as LSTM, which shows significant prediction deviation in the later stages, the BiGRU-QR model more accurately captures the uncertainty variations. The RMSE of the BiGRU-QR model is only 0.0157, the MAE is 0.0097, the MAPE is 0.6907, and the R^2 value reaches 0.9615, outperforming all other models and further demonstrating its superiority in handling uncertainty across different battery states. A similar performance was observed with the CALCE dataset, specifically for the CS2_35 battery. Throughout the entire charge-discharge cycle, the BiGRU-QR model, due to its structure and computational process, effectively captures and quantifies uncertainty. The RMSE is 0.0393, the MAE is 0.0292, the MAPE is 7.0077, and

the R^2 value is 0.9412, again outperforming the other comparative models, providing a more reliable basis for battery capacity prediction.

4. Conclusion

To enhance the accuracy of battery remaining lifespan predictions and to prevent performance degradation of lithium-ion batteries that could lead to equipment failures or catastrophic events, this study has developed a lifespan prediction method for lithium-ion batteries using DAE-CNN-BiGRU quantile regression. This model addresses the limitations of traditional point prediction methods by incorporating uncertainty expression for battery performance. The effectiveness of the model has been validated through experimental data, demonstrating an improvement in the accuracy of lithium-ion battery remaining lifespan predictions and providing a methodological foundation for ensuring the operational safety of lithium-ion batteries.

In this study, a comparative analysis of the fitted capacity degradation curves for the two battery datasets demonstrates that the prediction results of the CNN-BiGRU-QR model are the closest to the actual data. Residual boxplot analysis further confirms that the CNN-BiGRU-QR model exhibits the smallest prediction error with the most concentrated distribution. Additionally, across various evaluation metrics, the CNN-BiGRU-QR model consistently outperforms other models, achieving the lowest errors and the highest R^2 values. These findings validate the superiority of the CNN-BiGRU-QR model in the deterministic prediction of battery remaining useful life. Therefore, the method proposed in this study can significantly enhance the prediction accuracy of the remaining useful life of lithium-ion batteries, and also provides new insights and directions for future research on battery life prediction.

Acknowledgments

The authors acknowledge funding support from the Chongqing Natural Science Foundation under grant no. CSTB2024NSCQ-MSX0002 and CSTB2024NSCQ-MSX1204, the Science and Technology Research Program of Chongqing Municipal Education Commission under grant no. KJZD-K202400807.

References

[1] Z. Wei, J. Zhao, R. Xiong, G. Dong, J. Pou and K. J. Tseng, Online Estimation of Power Capacity With Noise Effect Attenuation for Lithium-Ion Battery [J], IEEE Transactions on Industrial Electronics, 2019, 66 (7):5724-5735.

[2] J. Zhang, H. Huang, G. Zhang, Z. Dai, Y. Wen and L. Jiang, Cycle life studies of lithium-ion power batteries for electric vehicles: A review [J], Journal of Energy Storage, 2024, 93:112231.

[3] J. Hong, D. Lee, E.-R. Jeong and Y. Yi, Towards the swift prediction of the remaining useful life of lithium-ion batteries with end-to-end deep learning [J], Applied Energy, 2020, 278:115646.

[4] Q. Liu, J. Zhang, K. Li and C. Lv, The Remaining Useful Life Prediction by Using Electrochemical Model in the Particle Filter Framework for Lithium-Ion Batteries [J], IEEE Access, 2020, 8:126661-126670.

[5] J. Sun, C. Tang, X. Li, T. Wang, T. Jiang, Y. Tang, S. Chen, S. Qiu and C. Zhu, A remaining charging electric quantity based pack available capacity optimization method considering aging inconsistency [J], eTransportation, 2022, 11:100149.

[6] A. Guha and A. Patra, State of Health Estimation of Lithium-Ion Batteries Using Capacity Fade and Internal Resistance Growth Models [J], IEEE Transactions on Transportation Electrification, 2018, 4 (1):135-146.

[7] L Chen, S Xie, AM Lopes, H Li, X Bao, C Zhang and P Li, A new SOH estimation method for Lithium-ion batteries based on model-data-fusion [J], Energy, 2024, 286 :129597.

[8] A. A. Hussein, Capacity Fade Estimation in Electric Vehicle Li-Ion Batteries Using Artificial Neural Networks [J],

IEEE Transactions on Industry Applications, 2015, 51 (3):2321-2330.

[9] H. Dai, G. Zhao, M. Lin, J. Wu and G. Zheng, A Novel Estimation Method for the State of Health of Lithium-Ion Battery Using Prior Knowledge-Based Neural Network and Markov Chain [J], IEEE Transactions on Industrial Electronics, 2019, 66 (10):7706-7716.

[10] J. Meng, G. Luo and F. Gao, Lithium Polymer Battery State-of-Charge Estimation Based on Adaptive Unscented Kalman Filter and Support Vector Machine [J], IEEE Transactions on Power Electronics, 2016, 31 (3):2226-2238.

[11] Y. Zhou, S. Wang, Y. Xie, X. Shen and C. Fernandez, Remaining useful life prediction and state of health diagnosis for lithium-ion batteries based on improved grey wolf optimization algorithm-deep extreme learning machine algorithm [J], Energy, 2023, 285:128761.

[12] X. Shu, G. Li, Y. Zhang, S. Shen, Z. Chen and Y. Liu, Stage of Charge Estimation of Lithium-Ion Battery Packs Based on Improved Cubature Kalman Filter With Long Short-Term Memory Model [J], IEEE Transactions on Transportation Electrification, 2021, 7 (3):1271-1284.

[13] P. Li, Z. Zhang, Q. Xiong, B. Ding, J. Hou, D. Luo, Y. Rong and S. Li, State-of-health estimation and remaining useful life prediction for the lithium-ion battery based on a variant long short term memory neural network [J], Journal of Power Sources, 2020, 459:228069.

[14] L. Ren, J. Dong, X. Wang, Z. Meng, L. Zhao and M. J. Deen, A Data-Driven Auto-CNN-LSTM Prediction Model for Lithium-Ion Battery Remaining Useful Life [J], IEEE Transactions on Industrial Informatics, 2021, 17 (5):3478-3487.

[15] J. Mou, Q. Yang, Y. Tang, Y. Liu, J. Li and C. Yu, Prediction of the Remaining Useful Life of Lithium-Ion Batteries Based on the 1D CNN-BLSTM Neural Network [J], Batteries, 2024, 10 (5):152.

[16] X Bao, L Chen, AM Lopes, X Li, S Xie, P Li and Y Chen, Hybrid deep neural network with dimension attention for state-of-health estimation of Lithium-ion Batteries [J], Energy, 2023, 278 :127734.

[17] J. Liu, Q. Duan, K. Qi, Y. Liu, J. Sun, Z. Wang and Q. Wang, Capacity fading mechanisms and state of health prediction of commercial lithium-ion battery in total lifespan [J], Journal of Energy Storage, 2022, 46:103910.

[18] Q. Zhai, J. Sun, Y. Shang and H. Wang, A novel remaining useful life prediction method based on gated recurrent unit network optimized by tunicate swarm algorithm for lithium-ion batteries [J], Transactions of the Institute of Measurement and Control, 2024:01423312241257305.

[19] Y. Yu, C. Hu, X. Si, J. Zheng and J. Zhang, Averaged Bi-LSTM networks for RUL prognostics with non-life-cycle labeled dataset [J], Neurocomputing, 2020, 402:134-147.

[20] C Zhang, S Zhao, Z Yang and Y He, A multi-fault diagnosis method for lithium-ion battery pack using curvilinear Manhattan distance evaluation and voltage difference analysis [J], Journal of Energy Storage, 2023, 67 :107575.

[21] X. Guo, K. Wang, S. Yao, G. Fu and Y. Ning, RUL prediction of lithium ion battery based on CEEMDAN-CNN BiLSTM model [J], Energy Reports, 2023, 9:1299-1306.

[22] J. Zhang, C. Huang, M. Y. Chow, X. Li, J. Tian, H. Luo and S. Yin, A Data-Model Interactive Remaining Useful Life Prediction Approach of Lithium-Ion Batteries Based on PF-BiGRU-TSAM [J], IEEE Transactions on Industrial Informatics, 2024, 20 (2):1144-1154.

[23] K. Lv, Z. Ma, C. Bao and G. Liu, Indirect Prediction of Lithium-Ion Battery RUL Based on CEEMDAN and CNN-BiGRU [J], Energies, 2024, 17 (7):1704.

[24] T. Xia, X. Zhang, H. Zhu, X. Zhang and J. Shen, An accurate denoising lithium-ion battery remaining useful life prediction model based on CNN and LSTM with self-attention [J], Ionics, 2023, 29 (12):5315-5328.

[25] LI C, LI G, WANG K, et al. A multi-energy load forecasting method based on parallel architecture CNN-GRU and transfer learning for data deficient integrated energy systems [J]. Energy, 2022, 259: 124967.

[26] Z. Zhang, H. Qin, Y. Liu, L. Yao, X. Yu, J. Lu, Z. Jiang and Z. Feng, Wind speed forecasting based on Quantile Regression Minimal Gated Memory Network and Kernel Density Estimation [J], Energy Conversion and Management, 2019, 196:1395-1409.